Modeling and performance evaluation of in-line Fabry-Perot photothermal gas sensors with hollow-core optical fibers

HAIHONG BAO,[1,2] YINGZHEN HONG,[1,2] WEI JIN,[1,2,*] HOI LUT HO,[1,2] CHAO WANG,[1,4] SHOUFEI GAO,[1] YINGYING WANG,[3] (iD) AND PU WANG[3]

[1]*Department of Electrical Engineering, The Hong Kong Polytechnic University, Hung Hom, Kowloon, Hong Kong, China*
[2]*Photonic Sensors Research Center, The Hong Kong Polytechnic University Shenzhen Research Institute, Shenzhen 518057, China*
[3]*Beijing Engineering Research Centre of Laser Technology, Institute of Laser Engineering, Beijing, University of Technology, Beijing 100124, China*
[4]*School of Electrical Engineering and Automation, Wuhan University, Wuhan 430072, China*
[*]*wei.jin@polyu.edu.hk*

Abstract: We study photothermal phase modulation in gas-filled hollow-core optical fibers with differential structural dimensions and attempt to develop highly sensitive practical gas sensors with an in-line Fabry-Perot interferometer for detection of the phase modulation. Analytical formulations based on a hollow-capillary model are developed to estimate the amplitude of photothermal phase modulation at low modulation frequencies as well as the -3 dB roll-off frequency, which provide a guide for the selection of hollow-core fibers and the pump modulation frequencies to maximize photothermal phase modulation. Numerical simulation with the capillary model and experiments with two types of hollow-core fibers support the analytical formulations. Further experiments with an Fabry-Perot interferometer made of 5.5-cm-long anti-resonant hollow-core fiber demonstrated ultra-sensitive gas detection with a noise-equivalent-absorption coefficient of 2.3×10^{-9} cm^{-1}, unprecedented dynamic range of 4.3×10^{6} and <2.5% instability over a period of 24 hours.

1. Introduction

Photothermal interferometry (PTI) is a highly sensitive spectroscopic technique for trace-gas detection. PTI typically uses a pump-and-probe configuration: pump absorption of gas molecules generates localized heating, modulating the refractive index (RI) of gas-phase material and hence the phase of a probe beam propagating in the material. The photothermal (PT) phase modulation is proportional to the concentration of absorptive molecules and can be detected by using optical interferometry [1]. Recently, all-fiber gas detection with PTI has been demonstrated with a hollow-core photonic crystal fiber (HC-PCF) as the sensing element [2]. A HC-PCF confines gas-phase material, pump and probe light fields simultaneously in the hollow-core, providing an ideal platform for efficient light-gas interaction over a long distance. The all-fiber system greatly extends the capability of PTI for remoted sensing and applications in harsh environment [3].

To develop practical optical fiber PTI sensors with high sensitivity, various interferometric schemes, including Mach Zehnder interferometer (MZI) [2,4], Sagnac interferometer (SI) [5,6] and Fabry-Perot interferometer (FPI) [7], have been examined for the detection of the PT phase modulation. With a MZI configuration, short-term noise-equivalent gas (acetylene) concentration down to low parts-per-billion (ppb) level has been demonstrated with 1 to 10 meters of HC-PCFs [2,5,6]. However, the operation point of the MZI is not stable over a longer term (e.g., an hour)

even with a servo-control loop, making the system difficult for practical field applications. A SI could achieve better stability since the phase difference between the two counter-propagating waves in the same fiber is detected, which is relatively insensitive to low-frequency environmental perturbations. However, the differential phase detection could also mean lower sensitivity to PT phase modulation. To achieve high sensitivity detection of PT phase modulation, which is typically in the frequency range from a few to tens of kHz [5,6], many kilometers of single mode fiber (SMF) is required to form the Sagnac loop, which in turn increases the system noise.

A single fiber low-finesse FPI can be formed by natural reflections at the joints between hollow-core fiber (HCF) and SMFs, as illustrated in Fig. 1. Absorption of the modulated pump by gas molecules produces PT phase modulation, which is detected by the low-finesse FPI operating at the probe wavelength. The FPI detection scheme enables very compact sensing configuration as well as better immunity against environmental perturbation since the SMFs are merely used for light transmission and would not affect the stability of the interferometer. Low frequency external perturbation on the SMF has minimal effect on the PT phase detection since the reflected probe beams pass through the SMF almost at the same time (e.g., the time difference is less than 1 ns for 15 cm long sensing HCF) and hence the two beams basically experience the same perturbation and hence the differential difference is insensitive to the perturbation.
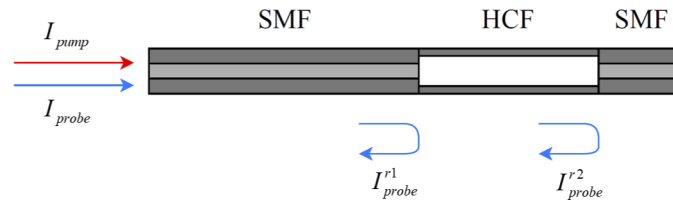
Fig. 1. Schematic of the FPI for PT gas detection with a hollow-core fiber. The pump and probe beam are copropagating in the HCF. I_{probe}^{r1} and I_{probe}^{r2} are the reflected probe beams.

In this article, we focus on PT gas sensing with FPI for phase detection and study issues to achieve high sensing performance including modeling and selection of HCFs and pump modulation frequencies to maximize PT phase modulation, demonstration of stable operation via servo-control of FPI operation point, testing of the system performance in terms of noise-equivalent gas concentration, dynamic range, response time and long term stability, and comparing with previously reported PT gas detection systems.

2. Optimizing PT phase modulation in hollow-core fibers

Different types of HCFs such as HC-PCFs and anti-resonant hollow-core fibers (AR-HCFs) may be used for PT gas detection [2,4–9]. Understanding PT phase modulation dynamics in these fibers with varying structural parameters is important for the design of sensors with optimal performance. In this section, we report a simple analytical model to estimate the amplitude as well as the roll-off frequency of PT phase modulation for a giving HC-PCF. The model is based on a simple gas-filled capillary and the results are compared with the more accurate numerical simulation using COMSOL Multiphysics and verified experimentally with a real HC-PCF and AR-HCF.

2.1. Analytical model

The dynamics of PT phase modulation in a gas-filled HCF has a complex dependence on the size and geometry of the HCFs, the mode fields of the pump and the probe beams as well as the absorption and thermal properties of gases in the hollow-core. However, we find that the magnitude as well as the -3 dB roll-off frequency of the PT phase modulation may be estimated

analytically with a simple gas-filled capillary model. Several approximations are made to simplify the analysis: (a) the gas absorption is weak and the pump power can be regarded as unchanged along the propagating path, allowing us to analyze the problem with a 2D model shown in Fig. 2; (b) the thermal conduction is the dominant process of heat dissipation [6]; (c) the HCF guides mainly the fundamental mode with a radially symmetric Gaussian intensity profile. Under these conditions, the steady-state temperature distribution, corresponding to PT phase modulation at the low frequency limit, obeying the differential equation [10]:

$$\frac{1}{r}\frac{d}{dr}\left(r\frac{dT(r)}{dr}\right) + \frac{Q(r)}{k} = 0 \tag{1}$$

where k is the gas thermal conductivity, $Q(r)$ is volume heat source given by:

$$Q(r) = \alpha C P_{pump}/(\pi w_{pump}^2)\exp(-r^2/w_{pump}^2) \tag{2}$$

where α is gas absorption coefficient, C is gas concentration, P_{pump} is the power and w_{pump} is the mode field radius of the pump beam. The PT phase modulation accumulated over a round-trip of the FPI with a HCF of length of L may be expressed as [6]:

$$\Delta\phi = -\frac{4\pi(n_0-1)L}{\lambda_{probe}}\int_0^R \frac{(T-T_{abs})}{T_{abs}} * \exp(-r^2/w_{probe}^2)/(\pi w_{probe}^2) * 2\pi r dr \tag{3}$$

where n_0 is the gas RI, λ_{probe} is the wavelength and w_{probe} the mode-field-radius of the probe beam. T_{abs} is the ambient temperature. Under the condition that the pump and the probe wavelengths are not far from each other, we may approximate $w_{pump} = w_{probe} = w$. Given the boundary conditions: $T(r = R) = T_{abs}$ and, $\frac{dT}{dr}\big|_{r=R} = 0$, the steady state phase modulation may be analytically expressed as:

$$\Delta\phi = \frac{\alpha C P_{pump}(n_0-1)L}{k\lambda_{probe}T_{abs}}\left\{\mu_{Euler} + En[1,\frac{2R^2}{w^2}] + 2Ei[-\frac{2R^2}{w^2}] - 2Ei[-\frac{R^2}{w^2}] + ln[\frac{R^2}{w^2}]\right\} \tag{4}$$

where $\mu_{Euler} = 0.5772$ is a Euler constant, $En(n,x) = \int_1^\infty \frac{e^{-xt}}{t^n}dt$ and $Ei(x) = -\int_{-x}^\infty \frac{e^{-t}}{t}dt$. From Eq. (4), it clarifies that for HCFs with different radius R, the PT phase change is determined by the ratio of R to w. Though the peak amplitude of the volume heat source is inversely proportional to the w_{pump}^2 as shown in Eq. (2), contrary to the intuition, smaller mode field diameter (MFD) will not necessarily benefit the measurement of the PT phase change, because for HCFs with smaller MFD, generally, its physical radius of the core R decreases as well, and the ratio of R/w may not change much.

At a higher pump modulation frequency, the PT phase modulation would be reduced due to (i) thermal relaxation time of gas molecules that reduces the heating efficiency (Eq. (2)) by a factor $(1 + (2\pi f\tau)^2)^{1/2}$, (ii) slow gas thermal conduction that makes temperature modulation being unable to follow the heat source. In general, an analytic expression for $\Delta\phi$ as a function of modulatin frequency is difficult and the results could only be calculated numerically. However, for gases with small τ (i.e., $2\pi f\tau \ll 1$), the -3 dB roll-off frequency of PT phase modulation, corresponding to modulation amplitude dropping to half of its maximum value, may be estimated with high accuracy using a simple expression. Based on the thermal dynamic analysis presented in [10], the -3 dB roll-off frequency of the PT phase modulation may be estimated by:

$$f_{3dB} = \frac{2\ln(2)\beta}{R^2} \tag{5}$$

where $\beta = k/\rho C_P$ is the gas thermal diffusivity. k is the gas thermal conductivity, ρ the gas density and C_P the specific heat capacity.
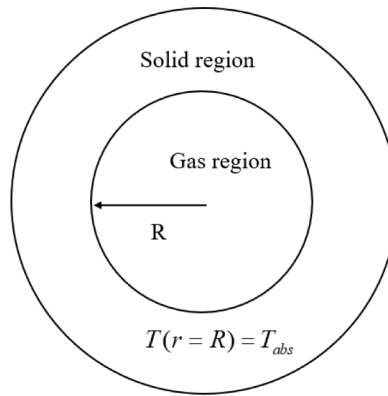
Fig. 2. A hollow capillary used as to model the gas-filled HCF.

2.2. Numerical computation

For practical applications, multi-component gas mixture is typically involved. The thermal conductivity k_m for the mixed gas may be obtained based on the equations in [11]. The gas density and specific heat capacity of the mixed gas may be determined by using $\rho_m = \sum C_i \rho_i$ and $C_{Pm} = \sum C_i C_{Pi}$, where C_i, ρ_i and C_{Pi} are the concentration, density and specific heat capacity of the ith gas component, respectively. Accordingly, the thermal diffusivity of the mixed gas may be expressed as: $\beta_m = k_m / \rho_m C_{Pm}$. However, it could be very difficult to predict the thermal relaxation time of the gas to be measured in a mixed gas environment. More molecular de-excitation paths may be provided by different gas components. The relaxation time of the targeted gas molecules may be calculated by following the analytical model in [12,13].

Based on the model in Fig. 2 and with the COMSOL Multiphysics software, we numerically computed the PT phase modulation for varying pump modulation frequency, capillary core radius and mode field radius. The pump and probe beams are assumed in the fundamental mode that has a Gaussian intensity profile in the hollow core. Hence the heating source is set as Gaussian distribution according to Eq. (2). The cladding material of the HCF is silica and the hollow region is filled with 1 ppm acetylene balanced in nitrogen. The gas pressure is 1 bar, and the environment temperature is set to be 293 K. The absorption coefficient of the acetylene is $1.16\,\mathrm{cm}^{-1}$. The thermal relaxation time of acetylene is 77 ns. The thermal diffusivity of the mixed gas is $2.1 \times 10^{-5}\,\mathrm{m}^2/\mathrm{s}$. The pump power is sinusoidally modulated at frequency f. Figure 3(a) shows the computed frequency-dependent PT phase modulation for a fixed R/w of 1.25. At low modulation frequencies (e.g., $f <$ 1kHz), the magnitudes of PT phase modulation are approximately the same for different capillary core radius, agreeing with the prediction that the steady-state phase modulation depends only on R/w. However, the roll-off frequency reduces from $\sim 0.9\,\mathrm{MHz}$ for $R = 5.5\,\mu\mathrm{m}$ to $\sim$10 kHz for $R = 50\,\mu\mathrm{m}$, agreeing with the prediction from Eq. (5). For a fixed mode field radius $w = 4.5\,\mu\mathrm{m}$, the magnitudes of PT phase modulation at low frequencies, determined by COMSOL Multiphysics and by Eq. (4), as function of capillary core radius R and the ratio of R/w are shown in Fig. 3(b). The PT phase modulation calculated using the two methods agree with each other and increases by $\sim$5 times for R from 5.5 to 40 μm. For the fixed R/w of 1.25, -3 dB roll-off frequency as function of R is shown in Fig. 3(c), the -3 dB roll-off frequencies determined by the two methods are very close, which decreases with increase core radius R.
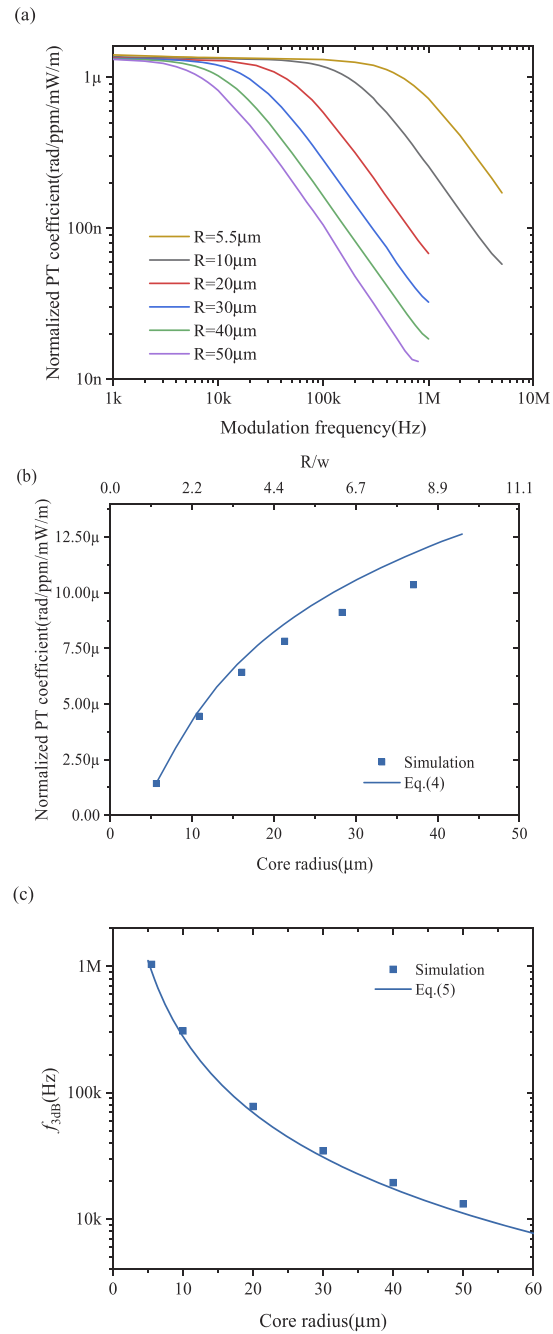
Fig. 3. (a) The calculated frequency-dependent PT modulation for HCFs with different core radius and with R/w fixed to 1.25. (b) The calculated PT phase modulation with $w = 4.5$ μm and the pump modulation frequency of 0.1 Hz. The dots are calculated using COMSOL Multiphysics while the line is the result from Eq. (4) with R/w raging from 1.25 to ~10. (c) The calculated -3-dB roll-off frequencies for HCFs with different core radius and with $R/w = 1.25$. The dots are calculated using COMSOL Multiphysics while the line is the result from Eq. (5) with 1 ppm acetylene balanced in air. The acetylene concentration of 1 ppm is used for computation in (a), (b) and (c).

2.3.   Experiments

Through a combination of theoretical analysis and numerical computation, it is found that larger PT phase modulation can be obtained using HCFs with a larger ratio of *R/w*. Here we experimentally test two types of HCFs with different *R/w* values. The first one is a HC-PCF (HC-1550-06 fibre from NKT Photonics) with cross-section shown in Fig. 4(a). The radius of the hollow core for this fiber is about 5.5 μm and the mode field radius is about 4.5 μm. The second one is an AR-HCF with cross-section shown in Fig. 4(b). This AR-HCF has an outer silica cladding with inner radius of 35 μm and 7 capillary rings with diameter of 17.5 μm and thickness of ~430 nm, which forms an inscribed air core with radius of ~17.5 μm.

(a)   (b)
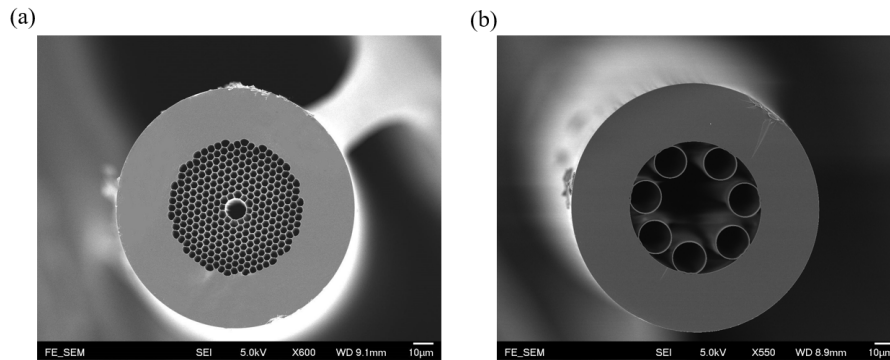
Fig. 4. The cross-sectional images of (a) the HC-1550-06 HC-PCF and (b) the AR-HCF.

The experiment setup is shown in Fig. 5. The sensing unit is made by fusion splicing one end of the HCF (HC-PCF or AR-HCF) to a SMF, while the other end is butt coupled to a SMF via ceramic sleeve and ferrules, which are fixed together by using ultraviolet (UV) curing glue. Natural reflections of the probe beam at the HCF/SMF joints form a low finesse FPI, which is used to detect PT phase detection. A micro gap is kept at the butt coupling joint for gas filling by diffusion. A section of the HCF is mounted on a piezoelectric transducer (PZT) to stretch the HCF to maintain the FPI operating at quadrature via servo control. The lengths of the FPI made by the HC-PCF and the AR-HCF are 4 cm and 5.5 cm, respectively.

The pump beam is from a 1.53-μm distributed feedback (DFB) laser. Its power is amplified by an erbium-doped fiber amplifier (EDFA) and intensity-modulated by an acoustic-optic modulator (AOM). At the same time, the wavelength of DFB laser is slowly scanned across the P(13) absorption line of acetylene at 1532.830 nm, which has the absorption coefficient is α=1.05/cm . The probe beam is an external cavity diode laser (ECDL) and its wavelength λ_{probe} is fixed at 1551.3 nm. The length of the HCF is tuned by the PZT so that FPI is always operating at quadrature at the probe wavelength. The pump and probe beams are combined through a 1550 nm/1530 nm wavelength-division multiplexer (WDM) and co-propagating in the HCF. The first harmonic (1*f*) component of the PT phase modulation is demodulated by the lock-in amplifier. The PT phase modulation is calibrated by a reference phase modulation produced by the PZT, by following a procedure described in Ref. [14].

The amplitude of modulation remains unchanged at low modulation frequencies and drops at higher modulation frequencies. The measured normalized frequency responses of PT phase modulation for the two fibers are presented in Fig. 6 as the red and blue dots, respectively. The -3 dB roll-off frequencies for the HC-PCF and the AR-HCF are ~750 kHz and ~34 kHz, respectively. Based on Eq. (5) we may define an effective heating dissipation radius R_e and they are 6.3 μm and 32 μm for the HC-PCF and the AR-HCF, respectively. By using the capillary model with radius of R_e, the frequency responses of the two fibers are calculated with
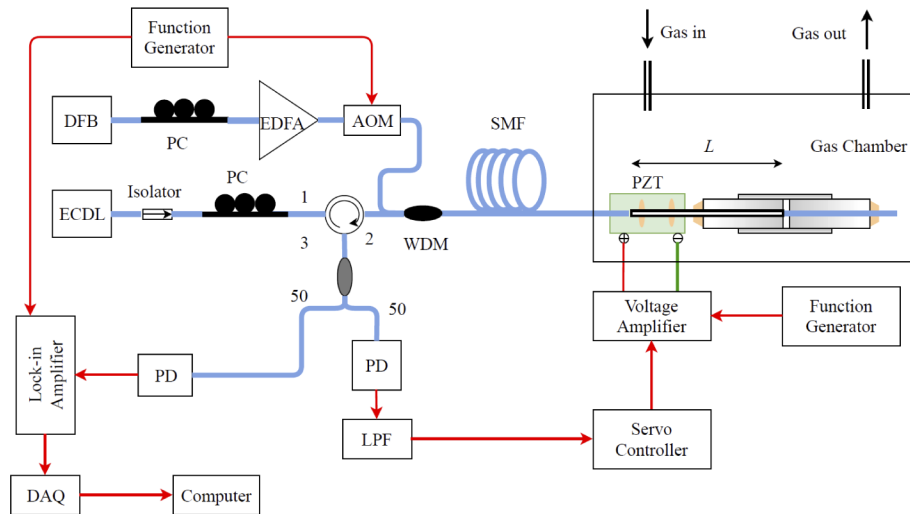
Fig. 5. Experimental setup to measure the frequency-dependent PT phase modulation of a HC-PCF and an AR-HCF. LPF: low pass filter which is used as part of the servo-loop for FPI stabilization; DAQ: data acquisition and PD: Photodetector.

COMSOL Multiphysics and shown as the solid red and blue lines in Fig. 6. It can be seen that the micro-structured inner silica cladding has significant influence on the measured PT phase modulation. For the HC-1550-06 fiber, the wall of the inner hollow core is connected to the solid outer cladding through a micro-structured silica web. The large air-filling fraction reduces speed of heating conduction into the surrounding silica, causing R_e being larger than physical radius of the inner hollow-core. However, the interconnected web maintains good thermal conduction (much better than air) and hence the R_e is only slightly larger than R, i.e., R_e=1.1 R. For the
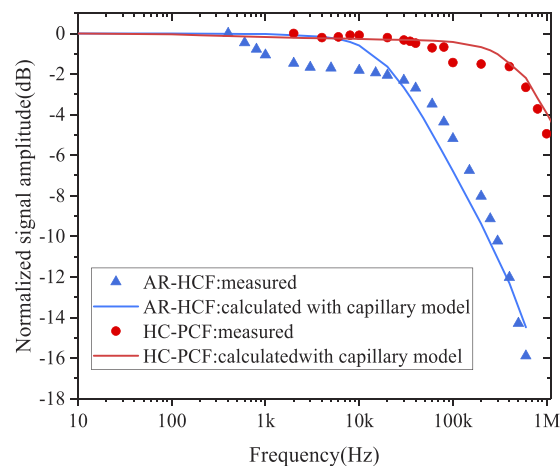

Fig. 6. The measured and calculated frequency response of PT modulation in AR-HCF and HC-PCF. The blue triangles are measured with the AR-HCF and the blue line is calculated using COMSOL Multiphysics based on the simplified capillary model with radius of the hollow core equals to 32 μm. The red dots are measured with the HC-PCF and the red line is calculated using COMSOL Multiphysics based on the simplified capillary model with radius of the hollow core equals to 6.3 μm.

AR-HCF, the capillary rings are not connected to each other and the contact area between the rings and the outer cladding is also small, making heating dissipation from the center of the core even less inefficient and leading to an even larger R_e=1.8R. Moreover, the deviation of the experimental result from that obtained from the simplified capillary model become larger in the frequency range from 1 to 20 kHz, indicating that the thermal conduction of the capillary region is considerably different from that of the solid silica model. The ratios of R_e/w for the HC-PCF and the AR-HCF are 1.4 and 2.56, respectively.

3. Gas detection with high sensitivity and stability

From last section, we understood that the AR-HCF has a larger R_e/w ratio, which enables larger PT phase modulation and hence better gas detection sensitivity at low pump modulation frequencies. In this section, we test the performance of the AR-HCF for gas detection. The experimental setup is shown in Fig. 7. This setup is basically the same as the one in Fig. 5, but instead of intensity modulation, the pump is wavelength modulated to achieve a higher signal-to-noise ratio (SNR), since harmonic detection at higher frequency may achieve lower system noise level. A 5.5 cm-long AR-HCF is used to form the FPI and the pump is modulated at 15 kHz. The FPI cavity length is locked to the probe laser so that it continuously operates at quadrature. The second harmonic ($2f = 30$ kHz) component of the probe phase modulation is demodulated by the lock-in amplifier.
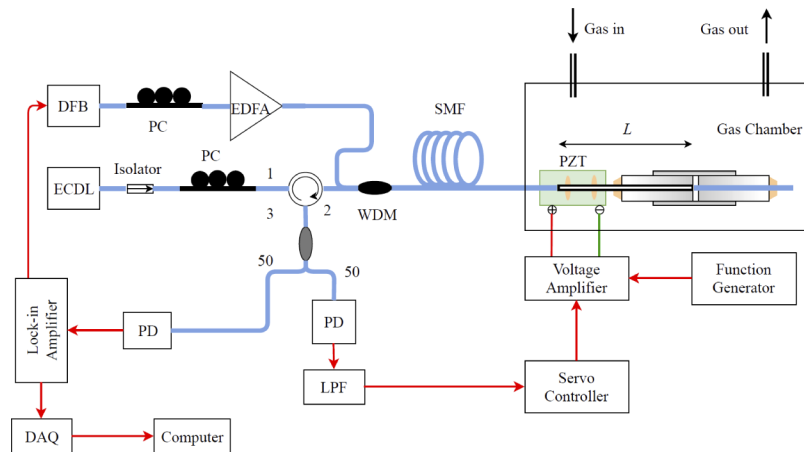

Fig. 7. Experimental setup for gas detection with PT spectroscopy in AR-HCF.

The experiments were firstly conducted with 1000 ppm acetylene balanced with nitrogen. Figure 8(a) shows the $2f$ lock-in output as the PT signal when the pump is scanned across the P(13) absorption line of acetylene with different pump power levels delivered into the AR-HCF. The system noise is estimated by tuning the pump wavelength off the absorption line and being fixed at 1532.5 nm. The PT signal amplitude increases linearly with pump power, while the standard deviation of the noise remains almost unchanged, as depicted in Fig. 8(b).
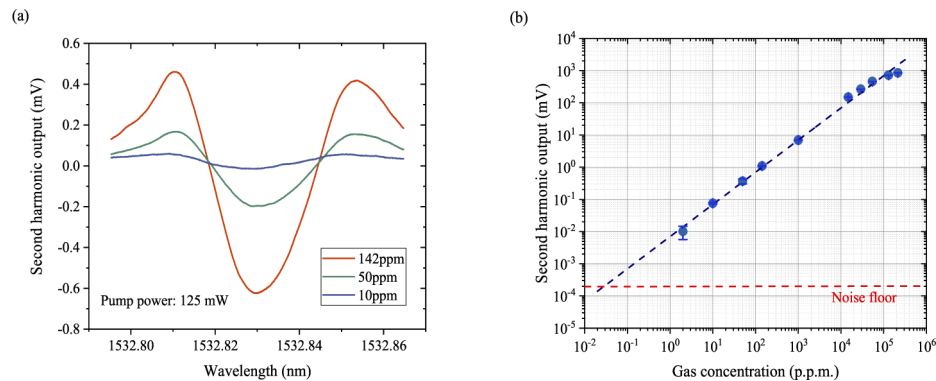
Figure 9(a) shows the PT signals for 10, 50 and 142 ppm acetylene in nitrogen with ~125 mW pump power delivered to the AR-HCF. Figure 9(b) shows the peak-to-peak amplitude of the PT signal as functions of acetylene concentration from 2 ppm to 21.3% acetylene in nitrogen. The noise floor in Fig. 9(b) is determined by measuring the standard deviation of the noise with pure nitrogen filled in the gas chamber. For a lock-in time constant of 1 second with a filter slope of 18 dB/Oct, the noise floor is ~0.22 μV, giving the noise-equivalent-concentration (NEC) of ~30 ppb for SNR of unity. An approximately linear relationship is obtained for acetylene
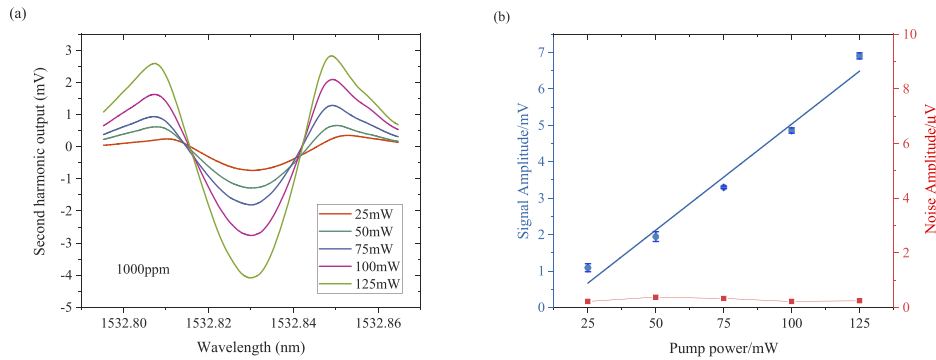
Fig. 8. (a) The measured PT signals with different pump power with a 5.5-cm-long AR-HCF. (b) The peak-to-peak value of the PT signal and the standard deviation (s. d.) of the noise as functions of pump power level with 1000 ppm acetylene balanced in nitrogen. Error bars show the s.d. of the PT signal from five measurements and the magnitudes of the error bars are scaled up by 10-fold for clarity reason.

concentration up to ~13% and non-linearity starts to appear beyond this value, giving a dynamic range of ~4.3×10^6, which is nearly an order of magnitude larger than the state-of-the-art gas detection systems [2].

Fig. 9. (a) Measured PT signals when pump laser is tuned across the P(13) absorption line of acetylene for 10, 50 and 142 ppm acetylene in nitrogen with ~125 mW pump power delivered to the AR-HCF. (b) Peak-to-peak amplitude of the PT signal as a function of gas concentration with ~125 mW pump power delivered to the AR-HCF. Error bars show the s.d. of the PT signal from five measurements.

Allan deviation analysis is conducted to investigate the stability of PT spectroscopy with the FPI made of the AR-HCF. Figure 10 shows the time trace and Allan plot of the baseline noise, which is recorded for 2 ppm acetylene in nitrogen recorded for 6 hours when the pump light is tuned away from the absorption line and fixed at 1532.5 nm. The pump power delivered to the AR-HCF is 125 mW. The optimal averaging time τ is determined to be ~670s, at which the s.d. of the noise level is 0.015 μV, corresponding NEC for an SNR of unity of 2.3 ppb. The NEC for 10 and 100 s averaging time are ~14 and 4.5 ppb, respectively

The signal stability is evaluated by monitoring the variation in the peak value of the PT signal when the pump wavelength is fixed to the peak of the P(13) absorption line of acetylene at 1532.83 nm. Figure 11 shows the time trace and the Allan plot of the relative fluctuation of the PT signal amplitude detected with 1000 ppm acetylene in nitrogen over 24 hours. The overall
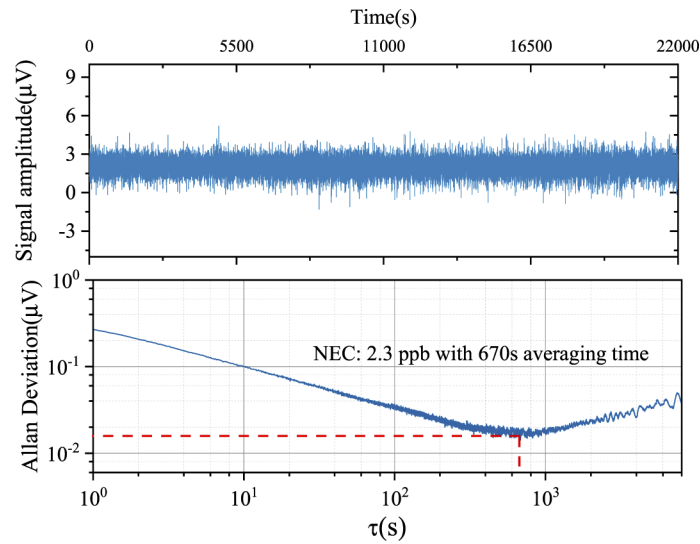
Fig. 10. Time trace (upper panel) and Allan deviation analysis (lower panel) of the baseline noise over a period of 6 hours. The time constant of the lock-in amplifier is 100 ms.

relative signal variation over 24 hours is ∼ 2.5%. With ∼800s averaging time, the relative signal variation is ∼4×10^{-6}.
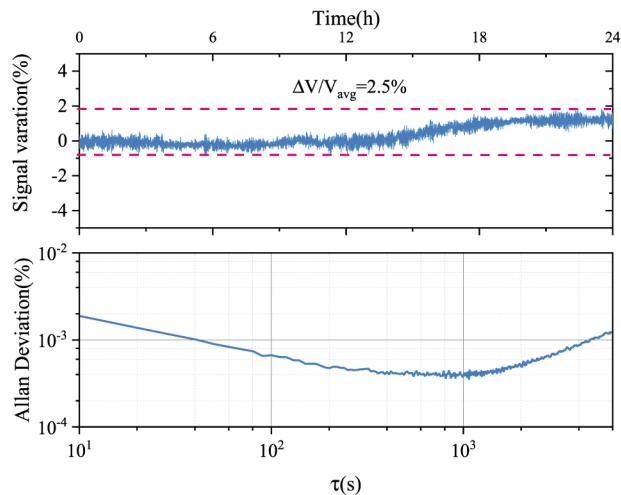
Fig. 11. The time trace (upper panel) and the Allan plot (lower panel) of the relative PT signal over 24 hours with 1000 ppm acetylene in nitrogen and 125 mW pump power in the AR-HCF. The time constant of the lock-in amplifier is 1 s.

Finally, the response time of the gas sensor is estimated by filling the gas chamber (12cmx3cmx2 cm) with acetylene in nitrogen. At first, the gas chamber is filled with atmospheric air. The pump wavelength is fixed at the center of the P(13) absorption line with ∼60 mW pump power delivered to the AR-HCF. At ∼10 s, pure acetylene mixed with pure nitrogen is filled into gas chamber with flow rate of ∼300 sccm. At ∼125s, the acetylene concentration reaches equilibrium. The mixed acetylene concentration is estimated to be ∼1100 ppm. At ∼135s, pure nitrogen is filled into the gas chamber with flow rate of ∼300 sccm. The measured 2f-signal as a function of time

during gas loading and unloading process is shown in Fig. 12. The response time $t_{90\%}$, which is defined as the time taken to reach 90% of the applied concentration, is ~52 s. Since the gas chamber volume is much larger than that of the hollow core, it would take much longer time to fill the gas chamber and reach a homogenous distribution of the acetylene. Hence, it is safe to conclude that the response time of the AR-HCF based gas sensor is less than 52s.
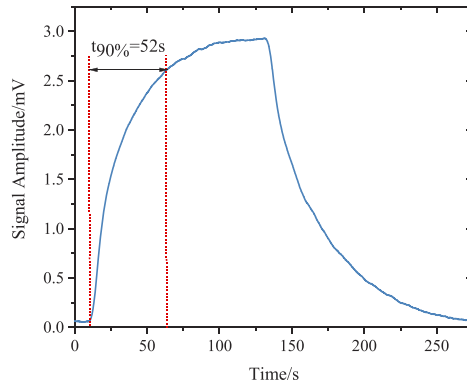
Fig. 12. The measured $2f$-signal as a function of time during gas loading and unloading process.

4.   Discussion

HCFs with a larger R_e/w ratio benefits gas detection for its larger PT phase modulation. The freedom to design HC-PCF with larger R_e/w is limited and in general R_e/w is only slightly larger than one. However, for AR-HCFs, it is possible to design the radius of the capillary rings to reduce the MFD of the fundamental mode but still keeping a large R_e, leading to a larger ratio of R_e/w. Further enhancement of PT phase modulation may be realized by optimizing the geometry of the AR-HCF to achieve a much larger ratio of R_e/w [15].

The PT phase modulation signal is linearly proportional to the pump power while the noise level remains nearly unchanged. Hence it is possible to further improve the detection limit by simply increasing the pump power level. The overlap between the fundamental optical mode and the silica in an AR-HCF is very small (<0.1%), which leads to a high damage threshold.

Table 1. Detection limit of some state-of-the-art gas sensors based HCFs

Gas type	Technique	HCF type	Wavelength /μm	Effective path length /m	NEA/cm^{-1}
Acetylene	PTI-MZI [2]	HC-PCF	1.53	10	2.3×10^{-9}
Acetylene	PTI-Sagnac Interferometer [5]	HC-PCF	1.53	1.1	2.1×10^{-8}
Acetylene	PTI-FPI [7]	HC-PCF	1.53	0.02	1.4×10^{-7}
Acetylene	Cavity-enhanced FPI [16]	HC-PCF	1.53	2.8	1.26×10^{-7}
Acetylene	Cavity-enhanced WMS [17]	HC-PCF	1.53	5.5	7×10^{-6}
Methane	WMS [18]	HC-PCF	1.65	0.14	2.5×10^{-4}
Nitrous oxide	PTI-MZI [9]	Capillary	4.46	0.25	2×10^{-5}
Carbon monoxide	PTI-MZI [4]	AR-HCF	2.32	0.85	3.2×10^{-6}
Acetylene	PTI-FPI (**This work**)	AR-HCF	1.53	0.05	2.3×10^{-9}

WMS: wave modulation spectroscopy.

Detection of sub-ppb-level acetylene with 1 s time constant is theoretically achievable by simply increasing the pump power.

The performances of some state-of-the-art gas sensors based on HCFs are summarized in Table 1. We use the noise-equivalent-absorption (NEA) which is independent of gas types and absorption strength to evaluate the detection sensitivity of different systems. The current work achieves best NEA among these HCF-based gas detection systems and with the shortest length of HCF.

5. Conclusion

Theoretical investigation based on a gas-filled capillary model shows that the PT phase modulation depends on the ratio of the capillary radius over mode field radius, i.e., R/w, with a larger ratio gives larger PT phase modulation at low modulation frequencies. Analytical expressions are derived to predict the amplitude of PT phase modulation at the low frequency limit as well as the -3-dB roll-off frequency. The AR-HCF has more freedom in achieve larger R/w and hence larger PT phase modulation. With a 5.5 cm-long AR-HCF gas cell and FPI for phase detection, ultra-sensitive PT gas sensors with excellent long-term stability is demonstrated. The extension of this technique to other wavelength bands (e.g., visible band and MIR band) is straightforward since AR-HCFs have broadband transmission windows.

Disclosures

The authors declare no conflicts of interest.

References

1. S. E. Bialkowski, *Photothermal Spectroscopy Methods for Chemical Analysis*, vol. 177. John Wiley & Sons, 1996.
2. W. Jin, Y. Cao, F. Yang, and H. L. Ho, "Ultra-sensitive all-fibre photothermal spectroscopy with large dynamic range," Nat. Commun. **6**(1), 6767 (2015).
3. B. Culshaw, G. Stewart, F. Dong, C. Tandy, and D. Moodie, "Fibre optic techniques for remote spectroscopic methane detection—from concept to system realisation," Sens. Actuators, B **51**(1-3), 25–37 (1998).
4. C. Yao, Q. Wang, Y. Lin, W. Jin, L. Xiao, S. Gao, Y. Wang, P. Wang, and W. Ren, "Photothermal CO detection in a hollow-core negative curvature fiber," Opt. Lett. **44**(16), 4048–4051 (2019).
5. Y. Lin, W. Jin, F. Yang, Y. Tan, and H. L. Ho, "Performance optimization of hollow-core fiber photothermal gas sensors," Opt. Lett. **42**(22), 4712–4715 (2017).
6. Y. Lin, Wei Jin, Fan Yang, Jun Ma, Chao Wang, Hoi Lut Ho, and Yang Liu, "Pulsed photothermal interferometry for spectroscopic gas detection with hollow-core optical fibre," Sci. Rep. **6**(1), 1–12 (2016).
7. F. Yang, Y. Tan, W. Jin, Y. Lin, Y. Qi, and H. L. Ho, "Hollow-core fiber Fabry–Perot photothermal gas sensor," Opt. Lett. **41**(13), 3025–3028 (2016).
8. Y. Lin, F. Liu, X. He, W. Jin, M. Zhang, F. Yang, H. L. Ho, Y. Tan, and L. Gu, "Distributed gas sensing with optical fibre photothermal interferometry," Opt. Express **25**(25), 31568–31585 (2017).
9. Z. Li, Z. Wang, F. Yang, W. Jin, and W. Ren, "Mid-infrared fiber-optic photothermal interferometry," Opt. Lett. **42**(18), 3718–3721 (2017).
10. C. C. Davis and S. J. Petuchowski, "Phase fluctuation optical heterodyne spectroscopy of gases," Appl. Opt. **20**(14), 2539–2554 (1981).
11. E. A. Mason and S. C. Saxena, "Approximate formula for the thermal conductivity of gas mixtures," Phys. Fluids **1**(5), 361–369 (1958).
12. M. Zhu, T. Liu, S. Wang, and K. Zhang, "Capturing molecular multimode relaxation processes in excitable gases based on decomposition of acoustic relaxation spectra," Meas. Sci. Technol. **28**(8), 085008 (2017).
13. T. Liu, S. Wang, and M. Zhu, "Predicting acoustic relaxation absorption in gas mixtures for extraction of composition relaxation contributions," Proc. R. Soc. London, Ser. A **473**(2208), 20170496 (2017).
14. F. Yang, W. Jin, Y. Lin, C. Wang, H. Lut, and Y. Tan, "Hollow-core microstructured optical fiber gas sensors," J. Lightwave Technol. **35**(16), 3413–3424 (2017).

15. S.-F. Gao, Y.-Y. Wang, W. Ding, and P. Wang, "Hollow-core negative-curvature fiber for UV guidance," Opt. Lett. **43**(6), 1347–1350 (2018).

16. Y. Tan, W. Jin, F. Yang, Y. Jiang, and H. L. Ho, "Cavity-enhanced photothermal gas detection with a hollow fiber Fabry-Perot absorption cell," J. Lightwave Technol. **37**(17), 4222–4228 (2019).

17. Y. Tan, W. Jin, F. Yang, H. L. Ho, and H. Kong, "High finesse hollow-core fiber resonating cavity for high sensitivity gas sensing application," J. Lightwave Technol. **35**(14), 2887–2893 (2017).

18. J. P. Carvalho, H. Lehmann, H. Bartelt, F. Magalhães, R. Amezcua-Correa, J. L. Santos, J. Van Roosbroeck, F. M. Araújo, L. A. Ferreira, and J. C. Knight, "Remote system for detection of low-levels of methane based on photonic crystal fibres and wavelength modulation spectroscopy," J. Sens. **2009**, 1–10 (2009).